ISBN: 978-93-48091-58-1

4. Influence of Ag Doping on Crystal Structure and Dielectric Properties of ZnO Compound

Bikash Dey[1,2]

[1]Department of Physics, Central Institute of Technology Kokrajhar, Kokrajhar,
[2]Department of Physics, Science College Kokrajhar, Kokrajhar, Assam.

Abstract:

The attempt to search for novel materials for optoelectronics material has become a highly debated and intensively investigated field of study. Within the scope of this investigation, Zn1−xAgxO (with x = 0 - 0.12) polycrystalline samples were produced using the traditional solid-state reaction method, and their crystalline structure and dielectric characteristics were investigated. The structural investigation through XRD technique suggesting that all the investigated samples are seen to crystallized in the hexagonal structure in addition to the secondary phase of metallic Ag. The Maxwell-Weigner model has been employed to fully understand how the dielectric constant (εr), loss tangent (tan δ), complex impedance, and ac conductivity of Ag doped ZnO compounds behave depending on frequency.

Keywords:

Ag doped ZnO, XRD, dielectric, ac conductivity.

4.1 Introduction:

In the past few decades, the extensive body of research demonstrates the rapid evolution of the field of spintronics and optoelectronics [ohono et al., 1998]. A frantic race has recently been motivated to find and create a new class of materials for use in optoelectronics involving fundamental research scientists and industrial partners. These devices operate better than conventional semiconductors in several respects, including higher storage capacity, faster data analysis, low power consumption, and non-volatility (Li et.al 2006).

Zinc oxide (ZnO) is considered to be one of the widely used oxide materials due to its wide range of uses, including photocatalysis, luminous material, solar cells, batteries, transducers, supercapacitors, biosensors, and biomedical devices in bulk crystal, thin film, and pellet form. It has a significant direct bandgap energy of 3.4 eV with wurtzite crystalline structure and 60 meV exciton binding energy at room temperature (Dung et a., 2016). Due to its wide optical band gap and high exciton binding energy, zinc oxide is a possible contender for applications in optoelectronics.

As a dopant, it can introduce specific energy levels into the host material's band structure, altering its electrical and optical properties. Similarly, silver (Ag) as a dopant in oxides has also received considerable attention. Silver nitrate ($AgNO_3$) is commonly used as a precursor source of silver due to its strong reactivity and stability. Because of these characteristics, $AgNO_3$ can be used in various chemical reactions, including solid-state route

processes (Shittu et al., 2023). For an ideal doping concentration range of 6 to 9%, Ag-doped SnO_2 compounds exhibited several intriguing physical (optical, magnetic, and transport) features in a recent work by Chouhan et al., 2021. In this work, we have studied the crystal structure and dielectric properties of $Zn_{1-x}Ag_xO$ (with x = 0 - 0.12) samples prepared by using conventional solid-state reaction method.

4.1 Experimental Techniques:

The $Zn_{1-x}Ag_xO$ (with x = 0 - 0.12) compounds was prepared by conventional solid state reaction technique. For the preparation of the sample, commercial high purity (99.99%) ZnO powder and $AgNO_3$ with 99.9999% purity (purchased from Alfa Aesar) were used as a starting material.

The quantity of starting compounds was weighted using a chemical balance in the estimated stoichiometry ratio. The weighed chemicals were then crushed/ground in dry conditions and then added acetone (in wet conditions) for homogenous mixing using an agate mortar and pestle. This ground powder was put in an alumina crucible and pre-sintered in the air for ten hours each at 200 °C and 300 °C, and for twenty hours at 500 °C in a programmed muffle furnace. It is to be mentioned here that $AgNO_3$ melts at 212 °C and it has a decomposition temperature of 250 °C.

Thus, the temperatures selected here for pre-sintering steps were appropriate so that Ag did not escape without combining. The pre-sintered powder was then compressed into cylindrical pellets with a diameter of 14mm and a thickness of 1mm using a hydraulic press at 4×10^5 Pa pressure.

These pellets were then sintered for additional 5 hours in the same furnace at optimal sintering temperatures to burn off the adhesive and other foreign particles and produce a densified composite. The XRD patterns was collected in the scattering angle (2θ) range of 20° to 80° and with a fine step size of 0.02 degrees to ascertain the synthesized materials' phase purity and crystalline structure. The dielectric properties of the material were performed with the help of LCR meter for the frequency from 100 Hz to 5 MHz at room temperature.

4.2 Results and Discussion:

4.2.1 Structure and Phase Analysis:

XRD measurements were used to analyze the crystalline structure or phase formation of Ag doped ZnO compounds and it is presented as Figure 4.1. Most significantly, all of the XRD peaks with mentioned (h k l) values corresponding to the hexagonal wurtzite structures (JCPDS 36-1451) of ZnO lattice. However, additional diffraction peaks are observed at 38.07°, 44.24° and 64.36° for all Ag-doped ZnO compounds. The observation of the secondary phase is likely to arises due to the unreacted Ag_2NO_3 compound. Also, it was observed that the Ag peaks (secondary phase) intensity increases as the amount of Ag doping percentage increases.

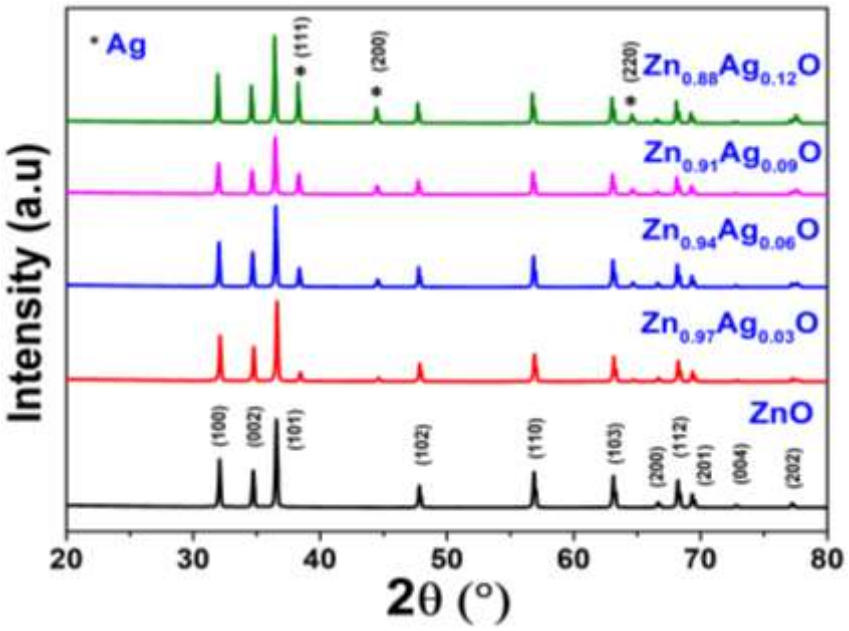

Figure 4.1: XRD pattern of $Zn_{1-x}Ag_xO$ compounds (x=0-0.12). Crystallographic planes are marked in the XRD of the undoped ZnO compound. The location of Ag peaks marked as *.

The XRD patterns of the synthesized samples were refined using the Pseudo-Voigt function in Fullprof software by employing Rietveld method (Deschamps et al., 2022) to extract further information like lattice parameters, cell volumes, size of crystallite, etc. Several parameters such as background, sample displacement, lattice constants, full width half maxima (FWHM), dimensional parameters, atomic locations, preferred orientations, and scale factors were all used to refine the XRD data. Figure 4.2(a), 4.2(b) display Rietveld refined XRD patterns of up-doped and 6% Ag doped ZnO samples.

Here, solid lines show calculated intensities, whereas red circles represent experimental data. The respective green and pink vertical bars just below the experimental and computed intensities reflect the possible peak locations of ZnO and Ag_2NO_3 as per Bragg's law. The subtracted intensity value of experimental data and refined data is shown in the bottom-most blue curve. The Rietveld analysis shows that the experimentally observed diffraction pattern matches extremely well with the software calculated intensities.

The refined cell parameters are obtained as a = b = 3.2548 Å and c = 5.2122 Å for undoped ZnO, which is consistent with other investigations (Chawla et al., 2009). Typically, there would have been an enlargement of cell volume and lattice parameters upon incorporation of a larger Ag^+ (1.26 Å) ion replaces a smaller Zn^{2+} (0.74 Å) ion. However, as compared to undoped ZnO, the refined XRD patterns for all the investigated compounds indicated no substantial change in cell parameters. The observed discrepancy in the cell volume and lattice parameters indicates that Ag^+ ions do not integrated into the host lattice and that typical kind of Ag:ZnO nanocomposite have formed.

The average crystallite size (S_c) of the specimens is determined using Debye- Scherrer's Formula (Shittu et al., 2023) for each one of the samples, taking into account of a few selected accentuated peaks, including (1 0 0), (0 0 2), (1 0 1), (1 0 2) and (1 1 0) at the relevant Bragg's angle:

$$S_c = \frac{k\lambda}{\beta \cos\theta}$$

Where S_c is the crystallite size to be evaluated, β is the FWHM belonging to the strongest peaks, θ is the Bragg's maxima peak angle, k is the Scherer's constant whose value has been set at 0.89 assuming the circular grains. For samples with x = 0, 0.03, 0.06, 0.08 and 0.12, the average crystallite sizes (S_C) were estimated to be 59, 68, 69, 70, and 90 nm respectively, indicating that Ag incorporation has increased the size of the crystallites in a regular manner.

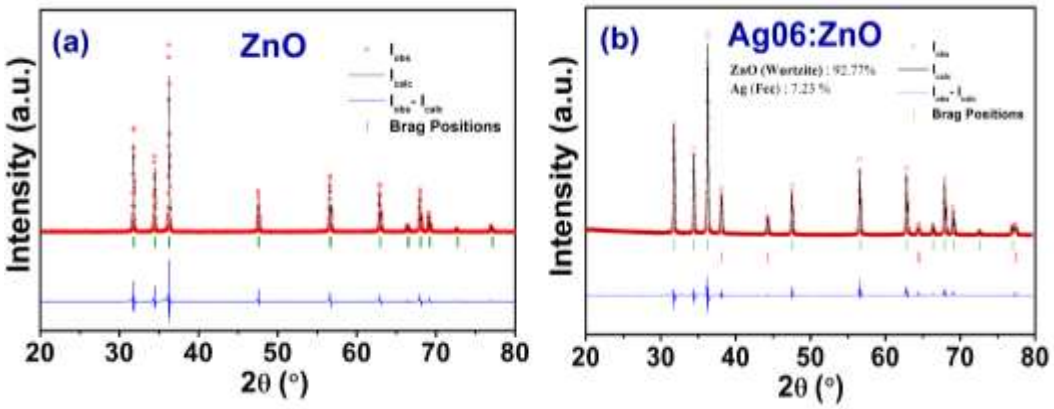

Figure 4.2: Rietveld refinement of XRD patterns for the (a) undoped ZnO (b) 6% Ag doped ZnO compound

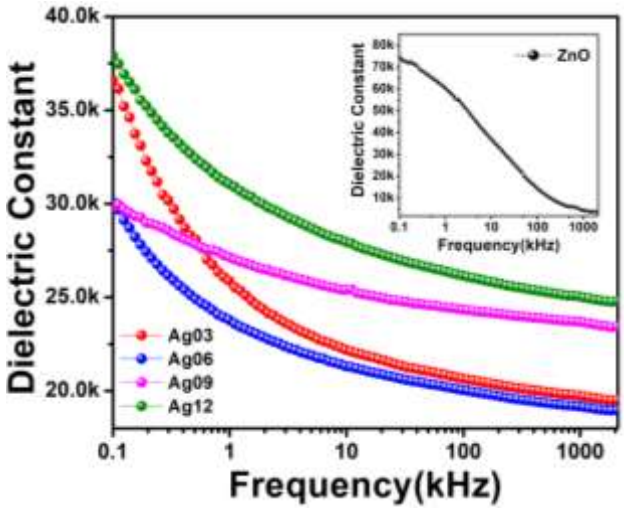

Figure 4.3: Plot of ε_r versus frequency for $Zn_{1-x}Ag_xO$ compounds at 300K.

4.2.2 Dielectric Analysis:

The dielectric analysis of the studied compounds at 300K was carried out through a phase multimeter or impedance analyzer meter over a wide band of frequency. In this study, we have investigated several frequency dependences of dielectric parameters which is elaborated in the next sections.

4.2.3 Dielectric Constant:

The variation of dielectric constant (ε_r) with frequency of the synthesized compounds $Zn_{1-x}Ag_xO$ (with x = 0 - 0.12) at 300 K are presented in Figure 4.3. It is noticed from the dielectric spectra that the ε_r values for both un-doped and Ag-doped ZnO compounds progressively decline with the enhancement of frequency, but they become almost constant in the high-frequency domain (>10 kHz). Thus, all the samples exhibit dielectric dispersion. It has been seen that in the low-frequency domain, the magnitude of ε_r for undoped ZnO is nearly double as compare to doped samples. However, it was seen that the value of ε_r drops when there is an increase in the amount of Ag doping percentage for the initial value (up to 6%), but then it rises again when there is a higher amount of Ag content. The dispersion associated with the Maxwell-Wagner Model (Wagner, 1973) correlates to the dramatic reduction in ε_r as frequency increases. According to the model, dielectric ceramics with resistant grain boundaries provide high resistance to the movement of charge carriers at low frequencies. Thus, the density of charge carrier at the grain boundaries is enhanced, which leads to an increase in the polarization of the space charges. With increasing frequency, the trapped charges at the grain boundaries scatter, and the carrier density begins to reduce, resulting in a decrease in ε_r value. Furthermore, a non-monotonic trend of reduction in ε_r with increasing Ag content was seen. Again, as per the curves, the ε_r values of the synthesized compounds tend to decrease when Ag is doped into the ZnO matrix.

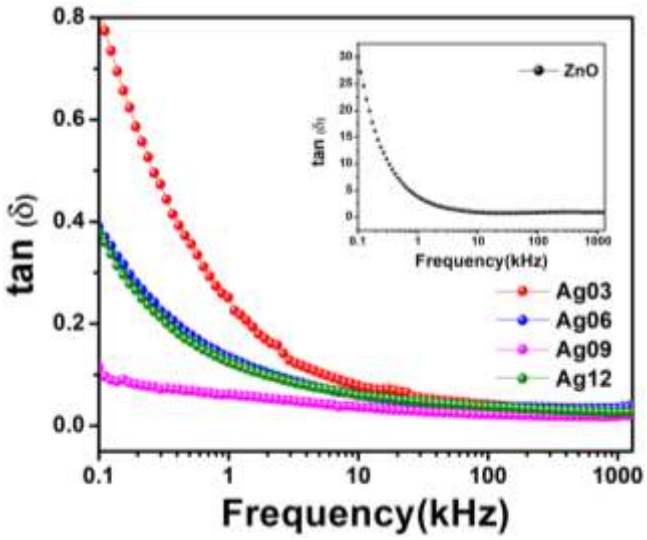

Figure 4.4: Plot of tanδ versus frequency for $Zn_{1-x}Ag_xO$ compounds at room temperature.

4.2.4 Dielectric Loss:

The frequency dependent variation of tanδ (loss factor) of the studied compounds $Zn_{1-x}Ag_xO$ (with x = 0 - 0.12) at 300K are presented in Fig. 4.4. It was noticed from the graph that the dielectric loss values for all the studied sample initially fall sharply with the rise in frequency, before showing a constant value of almost zero on the high-frequency side.

Such observed anomaly in the spectra tanδ can also be explained through Koop's phenomenological theory (Koops, 1951). As per the theory, the large value of tanδ at low frequency is owing to the strong resistivity supplied by grain boundaries and the high energy necessary for electron hopping, but the value drops towards high frequency because less energy is needed for electron hopping. Moreover, within the selected frequency range, no loss peak is visible in these materials. It may be attributed to dielectric permittivity contributing very little to loss factor's variation with frequency. These measurements, therefore, validated the Ag-doped compounds' lossless nature. As dielectric loss approaches to zero at high frequencies, these Ag-doped ZnO compounds could be suitable for use in high-frequency optoelectronic equipment.

4.2.5 Impedance Spectroscopy:

The complex impedance spectroscopy (CIS) is a very useful technique in order to correlate the electrical with microstructural features of the investigated material. This technique is capable of differentiate the contribution of electrode, grain and grain boundary effect in the overall impedance feature of the material. The frequency dependent variation of the real (Z') and imaginary (Z") component of impedance of the studied compounds $Zn_{1-x}Ag_xO$ (with x = 0 - 0.12) at 300K are presented in Fig. 4.5 and 4.6.

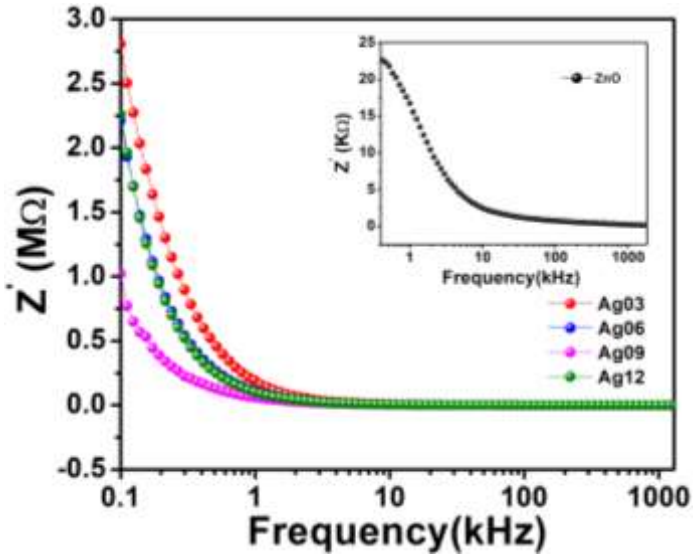

Figure 4.5: Plot of Z′ versus frequency for $Zn_{1-x}Ag_xO$ compounds at room temperature.

From the frequency dependent variation of Z', it was noticed that Z' varies quite in a sigmoid manner in the low-frequency zone whereas it becomes nearly saturated in the high-frequency zone. A similar response is seen in imaginary part of complex impedance versus frequency curves. Such observation once again clarifies the involvement of mixed polarization in the investigated system. The declining trend of Z' with increasing frequency for all the investigated samples attribute to the fall of density of trapped charges in the grain boundaries. On the high-frequency side, both Z′ and Z″ curves merge irrespective of Ag concentration was basically due to the ineffectiveness of space charge polarization at high frequency.

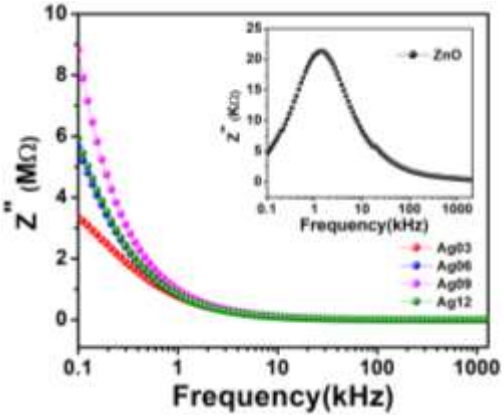

Figure 4.6: Plot of Z″ versus frequency for $Zn_{1-x}Ag_xO$ compounds at room temperature.

Figure 4.7 and its inset presents the Nyquist curves for Ag-doped ZnO and undoped compounds. Single depressed semicircular arcs are formed in the Nyquist plots for both undoped as well as doped samples. It is evident that as the doping percentage of Ag increases from 3 to 9%, the length of semi-circular arc rises, showing the resistivity of the compound increases, but an opposite trend, exhibiting the fall in electrical resistivity, as the concentration of Ag is raised to 12%. This hints that the dielectric relaxation is of non-Debye type behavior in these materials.

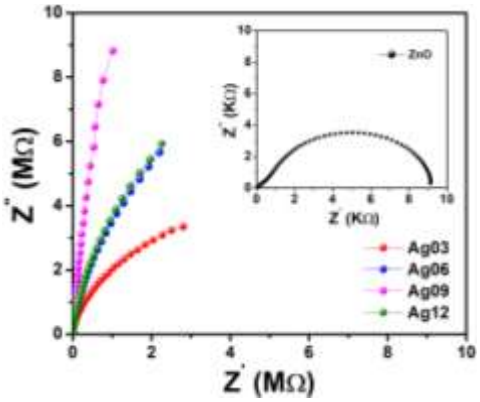

Figure 4.7: Nyquist plot for $Zn_{1-x}Ag_xO$ samples at room temperature.

4.2.6 AC Conductivity:

The frequency dependence of AC conductivity in the investigated compounds of $Zn_{1-x}Ag_xO$ (with x = 0 - 0.12) at 300K is depicted in Figure 4.8 In the low- frequency range, AC conductivity is seen to grow gradually, while at large frequency regions, both doped and undoped ZnO compounds exhibit a rapid increase in conductivity. In order to interpret the observed behavior of ac conductivity, the hopping model (Koops, 1951) can be utilized. Since the rate of charge carriers' hopping for transport is less at the lower frequency side, the conductivity value is low. However, for high-frequency ranges, the hopping of charges is improved with the enhancement of applied signal frequency, which increases their mobility. Thus, ac conductivity rises as charge mobility increases. Furthermore, as the concentration of Ag-doping raises, the value of ac conductivity falls. This occurs as a result of the appearance of silver ions introduces defects into the ZnO crystal lattice, including zinc interstitials, oxygen vacancies etc. Due of the diffusion mechanism, these defects seem to separate at the grain borders, promoting the formation of a grain boundary defect barrier, and limiting charge carrier transportation. Thus, Ag doping reduces the system's conductivity.

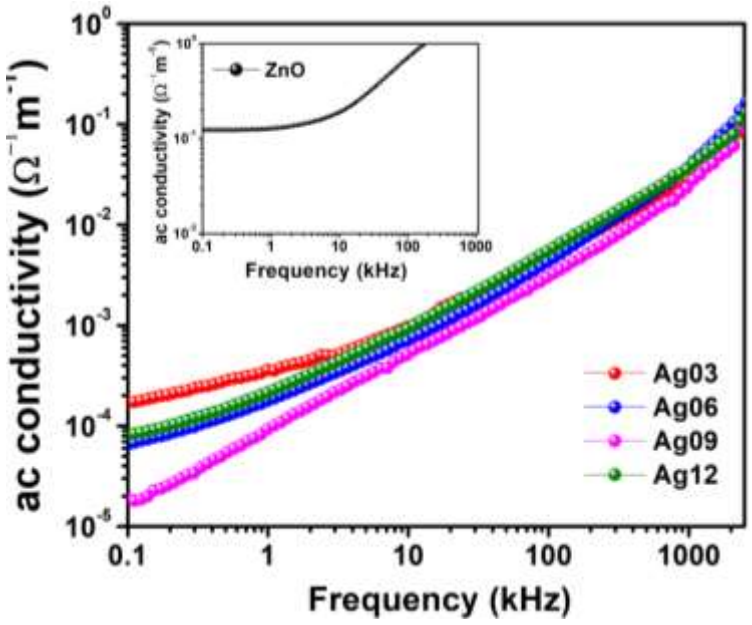

Figure 4.8: Plot of ac conductivity versus frequency for $Zn_{1-x}Ag_xO$ samples at room temperature.

4.3 Conclusion:

In this study, we have illustrated the detailed investigation of structural and dielectric properties of the Ag doped ZnO compounds. All the investigated samples were synthesized through the traditional solid-state reaction approach at appropriate sintering temperature. Based on the analysis of the XRD data, the investigated samples have been formed composite-like compounds.

The crystallite size lies within 85 to 95 nm as detected by XRD analyses. As per dielectric property study, the value of dielectric constant as well as ac conductivity found to be decreases with Ag doping percentage. Furthermore, the materials have negligible loss tangents at high frequencies. The synthesized materials are suggested to be suitable for optoelectronic, and high-frequency devices.

Declaration of Competing Interest:

The authors declare that they have no known competing financial interest personal relationships that could have appeared to influence the work reported in this paper.

4.4 References:

1. Ohno, Hideo. "Making nonmagnetic semiconductors ferromagnetic." *science* 281.5379 (1998): 951-956.
2. Li, Y., Qian, F., Xiang, J., & Lieber, C. M. (2006). Nanowire electronic and optoelectronic devices. *Materials today*, *9*(10), 18-27.
3. Theerthagiri, J., Salla, S., Senthil, R. A., Nithyadharseni, P., Madankumar, A., Arunachalam, P., ... & Kim, H. S. (2019). A review on ZnO nanostructured materials: energy, environmental and biological applications. *Nanotechnology*, *30*(39), 392001.
4. Dung, N. D., Son, C. T., Loc, P. V., Cuong, N. H., Kien, P. T., Huy, P. T., & Ha, N. N. (2016). Magnetic properties of sol-gel synthesized C-doped ZnO nanoparticles. *Journal of Alloys and Compounds*, *668*, 87-90.
5. Shittu, H. A., Adedokun, O., Kareem, M. A., Sivaprakash, P., Bello, I. T., & Arumugam, S. (2023). Effect of low-doping concentration on silver-doped SnO_2 and its photocatalytic applications. *Biointerface Res. Appl. Chem*, *13*(165.10), 33263.
6. Chouhan, L., Panda, S. K., Bhattacharjee, S., Das, B., Mondal, A., Parida, B. N., ... & Srivastava, S. K. (2021). Room temperature d^0 ferromagnetism, zero dielectric loss and ac-conductivity enhancement in p-type Ag-doped SnO_2 compounds. *Journal of Alloys and Compounds*, *870*, 159515.
7. Deschamps J.R., Flippen-Anderson J.L., Crystallography, in: Encyclopedia of Physical Science and Technology, Elsevier, 2002: pp. 121–153.
8. Chawla, S., Jayanthi, K., & Kotnala, R. K. (2009). High temperature carrier-controlled ferromagnetism in alkali doped ZnO nanorods. *Journal of Applied Physics*, *106*(11).
9. Wagner, K.W. (1973) The Distribution of Relaxation Times in Typical Dielectrics. *Annals of Physics*, 40, 817-819.
10. Koops, C. G. (1951). On the dispersion of resistivity and dielectric constant of some semiconductors at audiofrequencies. *Physical review*, *83*(1), 121.